[2] K. J. Parbhaker and B. C. Gregory, "Plane wave interaction with an inhomogeneous warm plasma column," *Can. J. Phys.*, vol. 49, pp. 2578–2588, 1971.
[3] H. Ikegami, "Scattering of electromagnetic waves from a plasma column in a rectangular waveguide," *Jap. J. Applied Physics*, vol. 7, pp. 634–645, June 1968.
[4] N. Okamoto, I. Nishioka, and Y. Nakanishi, "Scattering by a ferrimagnetic circular cylinder in a rectangular waveguide," *IEEE Trans. Microwave Theory Tech.*, vol. MTT-19, pp. 521–527, June 1971.
[5] G. Cicconi, V. Molinari, and C. Rosatelli, "Microwave reflection from a plasma column in a rectangular waveguide," *Jap. J. Applied Physics*, vol. 12, pp. 721–734, June 1973.
[6] R. F. Harrington, *Time Harmonic Electromagnetic Fields*. New York: McGraw-Hill, 1961.
[7] R. L. Bruce, F. W. Crawford, and R. S. Harp, "A reflection technique for plasma-density measurement," *J. Applied Phys.*, vol. 39, pp. 3349–3354, June 1968.
[8] G. M. Murphy, *Ordinary Differential Equations and their Solutions*. New York: Van Nostrand, 1960.
[9] G. N. Watson, *Theory of Bessel Functions*, 2nd ed. New York: Cambridge Univ. Press, 1944.
[10] P. M. Morse and H. Feshbach, *Methods of Theoretical Physics*, Part I. New York: McGraw-Hill, 1953.
[11] E. Cupini, V. Molinari, and P. Poli, "Reflection coefficient of an electromagnetic wave by a plasma column of variable electron density in a waveguide," *Alta Frequenza*, vol. XLII, pp. 62–68, Feb. 1973.
[12] R. F. Harrington, *Field Computation by Moment Methods*. New York: Macmillan, 1968.
[13] G. Cicconi and C. Rosatelli, "Alcuni Metodi di Calcolo Numerico in Problemi di Diffusione di Microonde da Ostacoli Cilindrici," *Alta Frequenza*, vol. XLII, pp. 41–51, Jan. 1973.
[14] A. P. Benedetti and P. Poli, "REFLEX: A programme to calculate the scattering by a plasma column in a rectangular waveguide," Comitato Naz. Energia Nucleare. RT/FIMA (75)3, 1975.

Some Effects of Field Perturbation upon Cavity-Resonance and Dispersion Measurements on MIC Dielectrics

P. H. LADBROOKE

Abstract—**An analysis is presented of field perturbations in MIC resonators in order to examine the errors which occur in permittivity measurements made by cavity-resonance methods: Q factor, coupling effects, fringing fields, crystal misalignment (for anisotropic materials), and changes in ambient temperature are all considered. Analysis of a cavity with mixed boundary conditions shows that the resonant-mode frequencies depend to the first order on that part of Q_0 associated with imperfect electric (metal) walls, but to the second order on that part associated with imperfect magnetic (open-circuit) walls. A new expression is given for the Q of an open-ended microstrip resonator when surface waves are excited in the dielectric, and it is shown that the unloaded Q (Q_0) can be dominated by this phenomenon. It is further shown that these Q-related effects, together with reactive perturbations arising from fringing and coupling structures, are the principal source of error in measurements for ε or ε_{eff}. Such reactive effects may be treated semiquantitatively by applying Slater's perturbation theorem to the affected region. These procedures lead to the following revised values for the crystal permittivity of sapphire (monocrystalline Al_2O_3) in the microwave region: $\varepsilon_{\|}$ (parallel to the c axis) = 11.6; $\varepsilon_{\perp}$ (base-plane) = 9.4.**

I. Introduction

ALTHOUGH alumina (ceramic Al_2O_3) finds more widespread application in hybrid microwave integrated circuits than does sapphire (monocrystalline Al_2O_3), sapphire offers the following advantages (against which one must offset its higher cost): i) its electrical properties are exactly repeatable from sample to sample; ii) it can be polished optically flat, which means that lower loss circuits of greater precision can be constructed by thin-film techniques; iii) it is transparent, so it is possible to align optically a "flipped" device chip for bonding directly into a microstrip circuit without the parasitic inductance of bond wires; iv) it is compatible with silicon epitaxial technology (SOS). Given these kinds of application, the need to measure the dielectric properties of either substrate material at microwave frequencies is clear.

A number of papers have been published dealing with test structures which can be made by thin-film metallizing the substrate itself, leading either to the permittivity ε directly [1]–[4], to an effective permittivity ε_{eff} in the case of microstrips [5], or to some secondary variation such as the temperature coefficient $(1/\varepsilon)(\partial\varepsilon/\partial T)$ [6]. All of these test circuits were, and still are, in the nature of cavity resonators with one dimension thin ($\ll\lambda$), often with mixed boundary conditions (i.e., some electric walls, some magnetic walls). The object was in every case to retrieve the permittivity from cavity-resonance measurements made upon the structure, using the relationship [7]

$$\varepsilon = \frac{c^2}{f_{n,m}^2}\left\{\left(\frac{n}{2y_1}\right)^2 + \left(\frac{m}{2z_1}\right)^2\right\} \tag{1}$$

Manuscript received February 17, 1976; revised December 3, 1976.
The author is with the Department of Solid State Electronics, University of New South Wales, Kensington, Australia 2033.

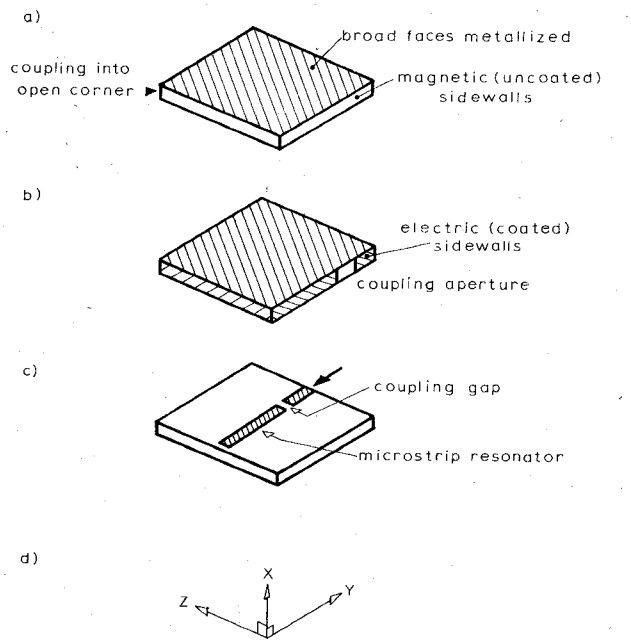

Fig. 1. Various types of resonators fabricated on a microwave integrated-circuit substrate.

where c is the velocity of light in vacuum; $f_{n,m}$ is the frequency of the (n,m)th resonant mode, and y_1 and z_1 are the principal dimensions of the cavity.

From the foregoing relationship it may be seen that an error $(\partial f/f)$ in f leads to an error $2(\partial f/f)$ in ε. It is the aim of this paper to enumerate the factors which disturb the frequencies from those given by the idealized model, (1) above, and to establish some principles of error correction so that ε can be determined to a known degree of accuracy. The types of resonators considered are those, shown in Fig. 1, having (in general) mixed boundary conditions consisting of imperfect electric and magnetic walls, together with at least one coupling port and, as noted earlier, one dimension thin, equal in fact to the thickness of the substrate itself.

II. Factors that Disturb the Resonances

In terms of normalized field quantities, as defined in Appendix A, Slater's perturbation theorem [8], [9]; viz.,

$$\frac{\omega^2 - \omega_a^2}{\omega_a^2} = \int_{\Delta\tau} (E_a^2 - H_a^2)\, dv \tag{2}$$

(where subscript a refers to the ath normal mode), states that either a change in the volume occupied by the cavity fields, or a change in the vector field within a given volume, or a combination of both, will cause the resonant frequency ω_a to shift. The theorem is of general applicability (see Appendix B for a proof that the theorem applies also for perturbations to magnetic sidewalls, not just electric walls as originally derived by Slater [8]). For the MIC resonators under consideration, there are four principal sources of such field perturbation.

a) An imperfection in one or more of the resonator walls which not only perturbs the fields locally but also admits an energy loss is one source of perturbation. (A cavity with lossy metal walls is an example.) For the purposes of this paper this type of perturbation is referred to as "Q_0-associated."

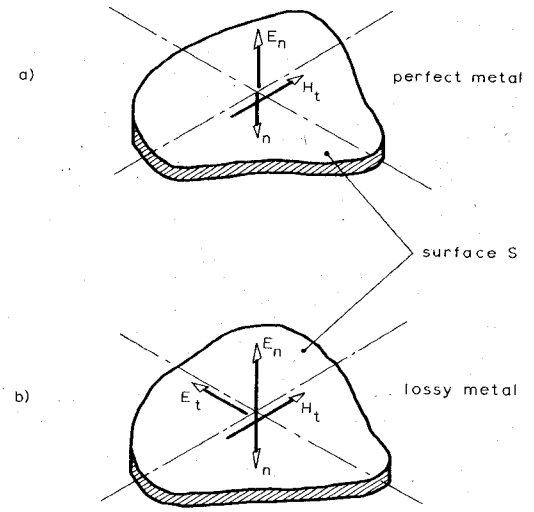

Fig. 2. Fields at perfect versus lossy metal walls. (a) Perfect conductor: E_n and H_t only. (b) Lossy conductor, i.e., $Z_m \neq 0$; an E_t appears.

b) An imperfection in one or more of the resonator walls which perturbs the fields, but where there is no associated energy loss that can be related to an unloaded Q factor (Q_0)—therefore a reactive-only effect—is another source. (An example is the so-called "fringing" approximation for the conditions which exist at the edge of an open-walled resonator or at the open end of a microstripline—see Fig. 1(a) and (c).)

c) Off-axis alignment of the dielectric substrate such that the crystal axes do not coincide with the resonator axes is a third source.

d) A change in the ambient temperature, which causes the resonator dimensions to change, the resistivity of the metallization to change, and the permittivity itself to change is a fourth source of perturbation.

We consider each in turn.

A. Q_0-Associated Perturbations

The standard calculation for the Q of a resonator bounded entirely by lossy metal walls has been given by Slater [8] and by Collin [7] among others. Fig. 2 summarizes the difference in the field systems existing at a perfect conductor and a lossy conductor. When the surface impedance Z_m, is nonzero and the walls are "imperfect electric," a tangential component of E appears at the surface, given by

$$\boldsymbol{n} \times \boldsymbol{E}_t = Z_m \boldsymbol{H}_t \tag{3}$$

where $\boldsymbol{n}$ is a normal directed into the surface and

$$Z_m = (1 + j)\sqrt{\frac{\omega\mu}{2\sigma}}. \tag{4}$$

μ and σ are, respectively, the permeability and conductivity of the metal. It is a well-known result that the frequency is then modified according to the formula [7], [8]

$$\omega \simeq \omega_a\left(1 - \frac{1}{2Q_0}\right). \tag{5}$$

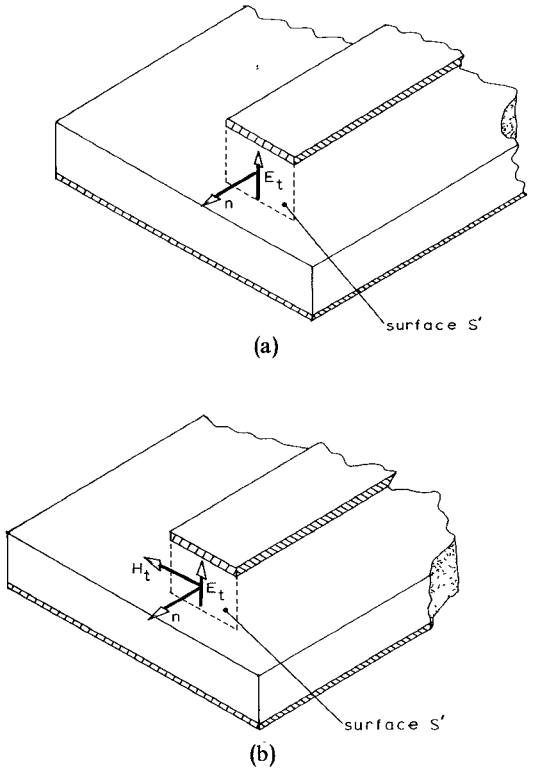

Fig. 3. Fields at perfect and imperfect open-circuit walls (microstrip resonator example). (a) Perfect end wall: only E_t exists at the wall. (b) Imperfect wall, i.e., $Y_d \neq 0$; there is no longer a node of H_t at the end of the microstrip.

In order to see how these results should be extended to the case of a resonator with one or more magnetic walls, we consider first of all the field conditions which exist at a perfect wall (Fig. 3(a)); $\boldsymbol{n} \times \boldsymbol{H} = 0$ at such a wall, i.e., there is no tangential $\boldsymbol{H}$ component. Fig. 3(a) shows, for example, this condition applied at the end of an open microstripline. In practice this state of affairs never exists and the wall is always lossy. It has been confirmed by a direct probing technique[1] [10] that when the strip actually terminates over the substrate so the dielectric and the ground plane extend beyond the end of the strip there is energy loss in the form of launched waves; a typical experimental result is shown in Fig. 4.[2] For a wave traveling away from the end wall [11], there arises a transverse magnetic field component given by

$$\boldsymbol{H}_t = Y_d \boldsymbol{n} \times \boldsymbol{E} \tag{6}$$

where $Y_d^{-1} = Z_{\text{free space}}/\sqrt{\varepsilon_r}$ is the wave admittance in the dielectric substrate (see Section III-A, where these fields are considered in more detail). There is therefore a component of tangential $\boldsymbol{H}$ at the wall whose existence is due to the fact that the wall is imperfect since it allows surface waves to be

[1] The circuit (or load) is printed on a very thin dielectric leaf so that it can be moved along the surface of the substrate proper (e.g., alumina), passing over a probe of special design etched into the ground plane.

[2] The field distribution shown in Fig. 4 is plotted directly by a Hewlett-Packard calculator which normalizes the experimental points to the standing-wave maximum.

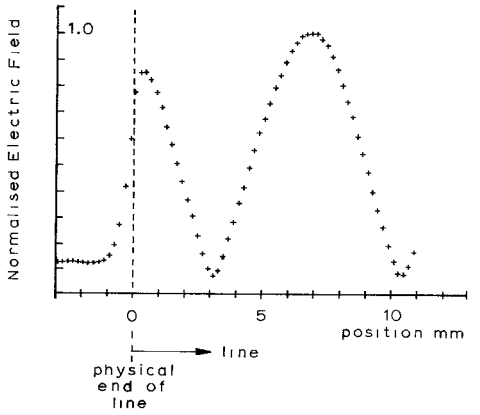

Fig. 4. Probed fields showing a standing wave in a microstrip resonator with a traveling-wave launched off the end into the substrate.

launched (Fig. 3(b) sketches these changes). Note that (6) is of the same form as (3). We now consider the calculation of how ω is modified in a resonator with both imperfect electric *and* magnetic walls, as represented, respectively, by the boundary conditions (3) over part of the resonator surface S, and (6) over the remainder of the resonator surface S'. The notation follows closely that used by Slater [8] (see Appendix A for a summary).

In terms of the coefficients $\int_V \boldsymbol{E} \cdot \boldsymbol{E}_a \, dv$ and $\int_V \boldsymbol{H} \cdot \boldsymbol{H}_a \, dv$ of the solenoidal field of components $\boldsymbol{E}_a$ and $\boldsymbol{H}_a$, Maxwell's curl equations become [8]

$$\nabla \times \boldsymbol{E} + \partial \boldsymbol{B}/\partial t = 0$$

$$k_a \int_V \boldsymbol{E} \cdot \boldsymbol{E}_a \, dv + \mu \frac{d}{dt} \int_V \boldsymbol{H} \cdot \boldsymbol{H}_a \, dv = -\int_S (\boldsymbol{n} \times \boldsymbol{E}) \cdot \boldsymbol{H}_a \, da \tag{7}$$

where V is the volume of the cavity.

$$\nabla \times \boldsymbol{H} - \partial \boldsymbol{B}/\partial t = \boldsymbol{J}$$

$$k_a \int_V \boldsymbol{H} \cdot \boldsymbol{H}_a \, dv - \varepsilon \frac{d}{dt} \int_V \boldsymbol{E} \cdot \boldsymbol{E}_a \, dv = \int_V \boldsymbol{J} \cdot \boldsymbol{E}_a \, dv - \int_{S'} (\boldsymbol{n} \times \boldsymbol{H}) \cdot \boldsymbol{E}_a \, da \tag{8}$$

where $k_a = \omega_a \sqrt{\mu\varepsilon}$ is the propagation constant for the ath resonant mode, and ω_a is the unperturbed frequency of that mode, i.e., the frequency that results when the boundary conditions are ideal. In place of these ideal conditions we have on S

$$\boldsymbol{n} \times \boldsymbol{E} = Z_m \boldsymbol{H} \tag{3}$$

on S'

$$\boldsymbol{H} = Y_d(\boldsymbol{n} \times \boldsymbol{E}) \quad \text{or} \quad (\boldsymbol{n} \times \boldsymbol{H}) = -Y_d \boldsymbol{E}. \tag{6}$$

Substituting (3) and (4) into (7),

$$k_a \int_V \boldsymbol{E} \cdot \boldsymbol{E}_a \, dv + \mu \frac{d}{dt} \int_V \boldsymbol{H} \cdot \boldsymbol{H}_a \, dv = -\int_S \boldsymbol{H} \cdot \boldsymbol{H}_a \, da(1+j) \sqrt{\frac{\omega\mu}{2\sigma}}. \tag{9}$$

Substituting (6) into (8) (with $J = 0$ throughout V),

$$k_a \int_V \boldsymbol{H} \cdot \boldsymbol{H}_a \, dv - \varepsilon \frac{d}{dt} \int_V \boldsymbol{E} \cdot \boldsymbol{E}_a \, dv = Y_d \int_{S'} \boldsymbol{E} \cdot \boldsymbol{E}_a \, dv. \tag{10}$$

If we now assume variations as $e^{j\omega t}$ where $\omega = \omega_1 + j\omega_2$ and that the coefficients $\int_V \boldsymbol{E} \cdot \boldsymbol{E}_a \, dv$ and $\int_V \boldsymbol{H} \cdot \boldsymbol{H}_a \, dv$ are suitably normalized to unity, we find

$$k_a \frac{\int_V \boldsymbol{E} \cdot \boldsymbol{E}_a \, dv}{\int_V \boldsymbol{H} \cdot \boldsymbol{H}_a \, dv} + j\omega\mu = -\frac{\int_S \boldsymbol{H} \cdot \boldsymbol{H}_a \, da}{\int_V \boldsymbol{H} \cdot \boldsymbol{H}_a \, dv} (1 + j) \sqrt{\frac{\omega_a \mu}{2\sigma}} \tag{11}$$

and

$$k_a \frac{\int_V \boldsymbol{H} \cdot \boldsymbol{H}_a \, dv}{\int_V \boldsymbol{E} \cdot \boldsymbol{E}_a \, dv} - j\omega\varepsilon = Y_d \frac{\int_{S'} \boldsymbol{E} \cdot \boldsymbol{E}_a \, da}{\int_V \boldsymbol{E} \cdot \boldsymbol{E}_a \, dv} \tag{12}$$

where, in the surface impedance root term in (11), we have recognized that ω must be real ($\simeq \omega_a$).

Combining these two equations to eliminate the first term on the left-hand side of each then yields, after collecting terms,

$$\begin{aligned} -\omega_a^2 \mu\varepsilon = {} & \left\{ \left[-\omega_2 \mu + A \sqrt{\frac{\omega_a \mu}{2\sigma}} \right] [-\omega_2 \varepsilon + Y_d B] \right. \\ & \left. - \omega_1 \varepsilon \left[\omega_1 \mu + A \sqrt{\frac{\omega_a \mu}{2\sigma}} \right] \right\} \\ & + j \left\{ \left[\omega_1 \mu + A \sqrt{\frac{\omega_a \mu}{2\sigma}} \right] [-\omega_2 \varepsilon + Y_d B] \right. \\ & \left. + \omega_1 \varepsilon \left[-\omega_2 \mu + A \sqrt{\frac{\omega_a \mu}{2\sigma}} \right] \right\} \end{aligned} \tag{13}$$

with

$$A = \frac{\int_S \boldsymbol{H} \cdot \boldsymbol{H}_a \, da}{\int_V \boldsymbol{H} \cdot \boldsymbol{H}_a \, dv} \tag{14}$$

$$B = \frac{\int_{S'} \boldsymbol{E} \cdot \boldsymbol{E}_a \, da}{\int_V \boldsymbol{E} \cdot \boldsymbol{E}_a \, dv}. \tag{15}$$

Equating real parts, and assuming for the present that ω_2 is so small that it can be neglected as an approximation, we find

$$-\omega_1^2 + \omega_a^2 - \omega_1 A \sqrt{\frac{\omega_a}{2\sigma\mu}} + A \sqrt{\frac{\omega_a}{2\sigma\mu}} \frac{Y_d B}{\varepsilon} \simeq 0. \tag{16}$$

If we now introduce the skin depth, $\delta = \sqrt{2/\omega_a \sigma \mu}$, we can show that

$$\sqrt{\frac{\omega_a}{2\sigma\mu}} = \frac{\omega_a \delta}{2}. \tag{17}$$

Inserting this into (16) then results in [8]

$$\frac{\delta A}{2} = \frac{\delta}{2} \frac{\int_S \boldsymbol{H} \cdot \boldsymbol{H}_a \, da}{\int_V \boldsymbol{H} \cdot \boldsymbol{H}_a \, dv} = \frac{1}{Q_s} \tag{18}$$

where Q_s is the unloaded Q factor due to loss at the metal walls as represented by the surface S. Similarly, we may show from the equations in Section III-A that

$$\frac{Y_d B}{\omega_a \varepsilon} = \frac{1}{Q_{s'}} \tag{19}$$

where $Q_{s'}$ is the unloaded Q factor due to energy lost from the resonator in the form of surface waves launched off the imperfect magnetic walls. With these Q factors, (16) becomes

$$-\omega_1^2 - \omega_1 \frac{\omega_a}{Q_s} + \omega_a^2 \left(1 + \frac{1}{Q_s Q_{s'}} \right) \simeq 0 \tag{20}$$

with the solution

$$\omega \simeq \omega_1 \simeq \omega_a \left\{ 1 - \frac{1}{2Q_s} \left[1 - \frac{1}{Q_{s'}} - \frac{1}{Q_s} \right] \right\} \tag{21}$$

which is a generalization of the well-known result, (5). (Note, however, that the last two terms on the right-hand side are second order, and as such they may not be the only second-order terms when ω_2 is included.)

The significance of (21) is that there is no *first-order* frequency pulling due to the fields arising from an imperfect magnetic wall of the type considered, provided that $Q_{s'} \gg 1$. There is, however, a *second-order* frequency shift which is similar to the pulling effect a lossy dielectric filling has on a cavity. The reason why metal walls are different in this regard is that the surface impedance (equation (4)) contains an inductive term, whereas the wave admittance (equation (6)) is entirely real in our approximation.

The second difficulty is that, if we are to correct ω for the effects of Q before inserting it into (1) for ε, we have to correct for Q_s as distinct from the unloaded Q factor Q_0, which ordinarily is the Q that is measured (after allowing for the effects of the external "load"):

$$\frac{1}{Q_0} = \frac{1}{Q_s} + \frac{1}{Q_{s'}}. \tag{22}$$

In Section III-A it will be shown that $Q_{s'}$ is entirely comparable to Q_s for a microstrip resonator, so the two must somehow be separated in practical cases where Q correction is considered important. It is clear from (21) and (1) that errors of the order of 1 percent may arise in ε if the effect is ignored (depending upon the Q_s of the mode excited), and that an erroneously high value for ε will result.

B. Perturbations Which Are Solely Reactive in Their Effect

For a stable, hard substrate material which is not subject to mechanical deformation, there are two main sources of reactive perturbation: local distortion of the cavity fields at coupling ports and at open edges (magnetic walls) where the fields "fringe." Their influence is less easy to quantify than the Q-associated type, nevertheless a semiquantitative estimate of their frequency-pulling effect can be obtained using Slater's perturbation theorem, (2).

Considering, as examples, the three resonators shown in Fig. 1, the fact that some waveguiding structure must be brought into close proximity to the cavity corner in Fig. 1(a) obviously will disturb the fields there. How, and to what

TABLE I
RELATIONS FOR $(\omega^2 - \omega_a^2)/\omega_a^2$ FOR VARIOUS WALL DISTORTIONS

WALL TYPE	$\Delta\tau$ negative (effective volume of resonator decreased)	$\Delta\tau$ positive (effective volume of resonator increased)
Electric	$\int_{\Delta\tau} (H_a^2 - E_a^2)\, dv$	$\int_{\Delta\tau} (E_a^2 - H_a^2)\, dv$
Magnetic	$\int_{\Delta\tau} (E_a^2 - H_a^2)\, dv$	$\int_{\Delta\tau} (H_a^2 - E_a^2)\, dv$

extent, depends upon the structure. In Fig. 1(b), on the other hand, the fields will already be perturbed by the aperture in the sidewall, and whether this perturbation is made worse or better clearly depends upon whether the coupling structure in part reestablishes the original (metallized all-over) boundary condition, or tends to draw the fields further out from the aperture. Likewise in Fig. 1(c), there is already reactance at the line end due to fringing, and the proximity of the feed microstrip brings about a further modification to those fields. The principle we are trying to establish is that, once the coupling port and the coupling structure are defined, then that whole rigid assembly is considered for the way in which it perturbs the *resonator* fields; that is, the boundaries of the resonator are now imagined to be distorted slightly so as to enclose this locally perturbed field, and the volume between this and the original resonator surfaces is taken as the volume $\Delta\tau$ in Slater's theorem.

It is possible for the resonance frequency either to increase or to decrease as a result of such local perturbations: it depends firstly on whether it is an electric wall or a magnetic wall which is affected, and secondly on whether the effective volume of the cavity (i.e., the total volume V occupied by the cavity fields) is increased slightly ($\Delta\tau$ positive) or decreased slightly ($\Delta\tau$ negative). Appendix B extends Slater's original calculation [8] to include magnetic walls, with the results shown in Table I.

The error that these frequency shifts lead to in ε may be found using (1). If the exact (ideal) frequency ω_a, when inserted into (1), yields the exact value for the permittivity ε, and if inserting the shifted value leads to a value $(\varepsilon + \delta\varepsilon)$, then we may write

$$\frac{\varepsilon - (\varepsilon + \delta\varepsilon)}{\varepsilon} = \left(\frac{1}{\omega_a^2} - \frac{1}{\omega^2}\right)\omega_a^2$$

or

$$-\frac{\delta\varepsilon}{\varepsilon} = \frac{\omega^2 - \omega_a^2}{\omega^2} \simeq \frac{\omega^2 - \omega_a^2}{\omega_a^2}. \tag{23}$$

Thus the fractional error in ε is the *negative* of the values listed in Table I.

To illustrate the use of these formulas, let us calculate the effect of fringing upon ω^2 and ε for an open-edged waveguide type of resonator, Fig. 1(a) (the calculation of errors due to coupling perturbations proceeds along exactly the same lines, and will be considered further in Section IV-B). In the absence of fringing, the electric field is everywhere zero outside the resonator, while inside the resonator it is given by

$$\boldsymbol{E} = \boldsymbol{a}_x \cos\frac{m\pi z}{z_1}\cos\frac{n\pi y}{y_1} \tag{24}$$

where y_1 and z_1 are the lengths of the resonator sides in the y and z directions, respectively (Fig. 1); for the moment we consider $m \neq 0$; $n \neq 0$. In the ideal case the lines of $\boldsymbol{H}$ at the open edges loop straight out normally (Fig. 5), and close in the space outside the resonator.

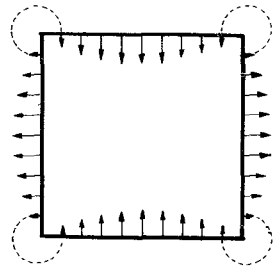

Fig. 5. Example of a magnetic field existing at the walls of an open-edged MIC resonator: (1,1) mode shown. (Arrows represent magnitude and direction of $\boldsymbol{H}$ at that point.)

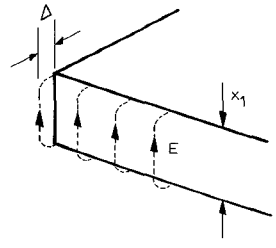

Fig. 6. Schematic of the fringing field at the open side wall of an MIC resonator.

When fringing occurs the magnetic field is negligibly different from the ideal case: the term "fringing" refers to the tendency for the electric field to loop out of the resonator edges, as shown in Fig. 6. We assume the fields do this by an amount Δ on all sides, so that we have, to good approximation,

$$\text{along the edges } y \lesssim 0 \quad \text{and} \quad y \gtrsim y_1\text{: } \boldsymbol{E} \simeq \boldsymbol{a}_x \cdot \cos\frac{m\pi z}{z_1} \tag{25}$$

$$\text{along the edges } z \lesssim 0 \quad \text{and} \quad z \gtrsim z_1\text{: } \boldsymbol{E} \simeq \boldsymbol{a}_x \cdot \cos\frac{n\pi y}{y_1}. \tag{26}$$

The integral in Slater's theorem (Table I, bottom right entry) then becomes (since $\boldsymbol{H}$ is unperturbed)

$$-\int_{\Delta\tau} E^2\, dv = -2\Delta x_1 \left\{\int_0^{z_1} \cos^2\frac{m\pi z}{z_1}\, dz + \int_0^{y_1} \cos^2\frac{n\pi y}{y_1}\, dy\right\}$$
$$= -2\Delta x_1 a \tag{27}$$

TABLE II

	Waveguide Resonators		Microstrip Resonators
	m≠0; n≠0	m=0 or n=0	(per end)
$\frac{\delta\varepsilon}{\varepsilon} = -\frac{\omega^2 - \omega_a^2}{\omega_a^2}$	$+\frac{4\Delta}{a}$	$+\frac{3\Delta}{a}$	$+\frac{\Delta}{a}$

where we have set $z_1 = a = y_1$. The normalization factor $2\int_V E^2\,dv$ [8], [9] must be calculated next:

$$2\int_V E^2\,dv = 2x_1\int_0^{z_1}\int_0^{y_1}\cos^2\frac{m\pi z}{z_1}\cos^2\frac{n\pi y}{y_1}\,dy\,dz = \frac{x_1 a^2}{2}. \tag{28}$$

Thus inserting

$$\int_{\Delta\tau} E_a^2\,dv = \frac{\int_{\Delta\tau} E^2\,dv}{2\int_V E^2\,dv} \tag{29}$$

into Slater's Theorem, there results

$$\frac{\delta\varepsilon}{\varepsilon} \simeq -\frac{\omega^2 - \omega_a^2}{\omega_a^2} \simeq -\int_{\Delta\tau} E_a^2\,dv = \frac{4\Delta}{a}. \tag{30}$$

For the case of a parallel-plate capacitor with the same dielectric outside the plates as inside, Plonsey and Collin [12] give a calculation for the fringing capacitance from which the following quantitative estimate for Δ (valid when the length of the edge at which fringing is taking place is very much greater than the plate spacing) may be obtained:

$$\Delta = \frac{x_1}{2\pi}\ln\frac{\pi a}{x_1} = 0.8x_1 \tag{31}$$

where we have used the typical dimensions for an MIC substrate of $x_1 = 0.5$ mm, $a = 25$ mm. When the dielectric inside the resonator has a value ε_r greater than that outside, (31) is generalized to (as an approximation)[3]

$$\Delta \simeq \frac{x_1}{2\pi\varepsilon_r}\ln\frac{\pi a}{x_1} = \frac{0.8x_1}{\varepsilon_r} \tag{32}$$

so that finally, given $\varepsilon_r \simeq 10$,

$$\frac{\delta\varepsilon}{\varepsilon} \simeq \frac{3.2x_1}{\varepsilon_r a} = +0.64 \text{ percent} \tag{33}$$

independently of the mode excited. The sign of this result is in accordance with intuitive expectation, and is contrary to a suggestion recently put forward by Owens *et al.* (see Appendix A of [13]). Table II contains further fringing results for other modes and resonators.

Note that in the case of the microstrip resonator, (32) could only be used as a very crude approximation for Δ. Nevertheless it is evident that, depending upon the detailed geometry of the cavity, fringing may lead to errors of the order of 1 percent in ε.

It has been found by experiment that coupling errors, as distinct from fringing errors, can be either positive or negative and, depending upon the sensitivity of the apparatus used to detect the resonances, can be up to 4 percent in magnitude [3]. As remarked earlier in connection with Table I, it depends upon whether $\boldsymbol{E}$ or $\boldsymbol{H}$ is disturbed as to whether a positive or negative error results. This matter is taken up again in Section IV-B.

C. Substrate Misorientation

Sapphire is a uniaxial crystal; it is therefore anisotropic. (There is also evidence to show that alumina can be anisotropic [6], [14].) Providing, however, that the principal axes of the crystal are aligned with the substrate (i.e., resonator) axes, the permittivity tensor is diagonal with two of the components the same, for instance,

$$[\varepsilon] = \begin{bmatrix} \varepsilon_{\parallel} & 0 & 0 \\ 0 & \varepsilon_{\perp} & 0 \\ 0 & 0 & \varepsilon_{\perp} \end{bmatrix} \tag{34}$$

where $\varepsilon_{\parallel}$ refers to the permittivity parallel to the c axis; $\varepsilon_{\perp}$, to the permittivity perpendicular to the c axis.

If the crystal axes do not coincide with the resonator axes, the off-diagonal terms in the tensor are nonzero, and in the specific case of the waveguide-type resonators we can show that the propagation must convert from TE to hybrid waves [15].

A first-order effect is the change that occurs in the tensor component ε_{xx}, and this has been used as a guide to the magnitude of the changes to be expected from crystal misorientation. It can be shown that if the permittivity components along the principal axes (x',y',z') are $\varepsilon_{x'}$, $\varepsilon_{y'}$, and $\varepsilon_{z'}$, respectively, and if the substrate (resonator) axes (x,y,z) are rotated out of coincidence with the crystal by an angle β about the y' axis and an angle α about the x' axis, then the tensor component along the resonator x axis becomes

$$\varepsilon_{xx} = \varepsilon_{x'}\cos^2\beta + \varepsilon_{y'}\cos^2\alpha\sin^2\beta + \varepsilon_{z'}\sin^2\alpha\sin^2\beta. \tag{35}$$

For example, for the x axis misaligned by $\alpha = \beta = 2°$, the change in ε_{xx} is about 0.05 percent (2° is a typical guaranteed orientation accuracy). Thus crystal misorientation contributes a small and insignificant error; it is worth noting, however, that it leads to an increase in the apparent value of $\varepsilon_{\perp}$ and a decrease in $\varepsilon_{\parallel}$.

D. Changes in Ambient Temperature

It has been shown in [6] that the temperature coefficient of resonance frequency is given by

$$\frac{1}{f}\frac{df}{dT} = -\frac{1}{2}\left(\frac{1}{\varepsilon}\frac{\delta\varepsilon}{\delta T} + \alpha_1 + \alpha_2\right) + \frac{1}{2Q_s^2}\frac{dQ_s}{dT} \tag{36}$$

where α_1 and α_2 are the expansion coefficients of the anisotropic crystal. (Note that we have replaced Q_0 by Q_s in

[3] This follows from the fact that the energy density inside the resonator increases by a factor of ε_r when the dielectric is introduced. Therefore, the *normalized* energy density in the region just outside the resonator is reduced by the same factor. An equivalent way of accounting for this reduction is to take Δ as given by (32).

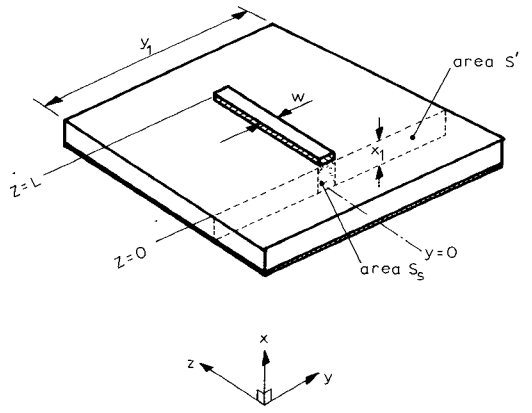

Fig. 7. Microstrip resonator.

the right-hand side of (36) since, as shown in Section II-A, f depends, to the first order, on Q_s, not Q_0.) For various types of resonators, including 50-Ω microstrip, it was shown that $(1/f)(df/dT)$ lies somewhere in the range

$$\frac{1}{f}\frac{df}{dT} = -(5.9 - 7.2)10^{-5} \text{ per degree K.}$$

Thus, if as an extreme case we imagine a 10°C difference in ambient temperature between two sets of measurements, we might expect an error of approximately 0.07 percent. This, too, is too small to be of any consequence in laboratory measurements.

In summary, it is clear from the analysis of Section II that the dominant sources of error are field perturbations at the *electric* (metal) walls which can be described in terms of an unloaded Q factor Q_s, coupling reactance, and parasitic reactance due to fringing fields. The significance of these findings for microstrip resonators and waveguide-type cavities is taken up in Sections III and IV below.

III. Microstrip Resonators

A. Correction of Q_0 for $Q_{s'}$

This kind of resonator has recently been used by Edwards *et al.* [5] for dispersion measurements on microstrips on sapphire, culminating in an effective permittivity parameter ε_{eff}. The need to correct the measured frequencies for Q_s requires that $Q_{s'}$ be separated somehow from Q_0. To this end we derive an expression for $Q_{s'}$ for the device shown in Fig. 7. The analysis proceeds by first estimating the transmission coefficient T which relates the power P_d carried by the surface wave launched from the end of the resonator into the dielectric to the power P_s carried by the wave in the strip, thus

$$P_d = TP_s \tag{37}$$

(such a calculation has already been outlined in [11] but a resumé is included here for completeness). The second part of the analysis is to calculate $Q_{s'}$ according to the usual definition

$$Q = 2\pi\left\{\frac{\text{total energy stored}}{\text{energy lost/cycle}}\right\}. \tag{38}$$

An expression for the power transmission coefficient T can be derived [11] by treating the field interaction at the line end as a wave-launching problem as done by Barlow and Brown [16]. It may be shown that the expression given by them applies equally to the present case, with the result that

$$T = \frac{1}{16P_sP_d}\left|\int_{S_s}(\boldsymbol{E}_s \times \boldsymbol{H}_d - \boldsymbol{E}_d \times \boldsymbol{H}_s)\cdot \boldsymbol{n}\, da\right|^2 \tag{39}$$

where

$\boldsymbol{n}$ is a normal to $S_s S'$, directed along $-z$.

The fields are approximated as follows.

In the microstrip, with effective relative permittivity ε_{eff},

$$\left.\begin{aligned}\boldsymbol{E}_s &= \boldsymbol{a}_x E_{sx}\\ \boldsymbol{H}_s &= -\boldsymbol{a}_y H_{sy}\end{aligned}\right\} \quad -\frac{w}{2} \le y \le +\frac{w}{2} \quad \begin{cases}0 < x < x_1\\ 0 < z < L.\end{cases} \tag{40}$$

In the dielectric, of relative permittivity ε_r (valid only for tightly bound waves [11]),

$$\left.\begin{aligned}\boldsymbol{E}_d &= \boldsymbol{a}_x E_{dx}\\ \boldsymbol{H}_d &= \boldsymbol{a}_y H_{dy} + \boldsymbol{a}_z H_{dz}\end{aligned}\right\}$$

$$-\frac{y_1}{2} < y < +\frac{y_1}{2} \quad \begin{cases}0 < x < x_1\\ z < 0.\end{cases} \tag{41}$$

The relationships between the transverse components are as follows:

$$\boldsymbol{H}_{st} = Y_s \boldsymbol{n} \times \boldsymbol{E}_{st} \tag{42}$$

$$\boldsymbol{H}_{dt} = -Y_d \boldsymbol{n} \times \boldsymbol{E}_{dt}. \tag{43}$$

(For the purpose of this calculation both waves are assumed to be traveling toward the interaction plane [16], hence the sign in (43) is reversed compared with (6).) Y_s and Y_d are the wave admittances in the strip and the dielectric, respectively:

$$\begin{aligned}Y_s &= Y_{\text{free space}}\sqrt{\varepsilon_{\text{eff}}}\\ Y_d &= Y_{\text{free space}}\sqrt{\varepsilon_r}.\end{aligned} \tag{44}$$

The power carried by the strip wave is given by

$$P_s = \tfrac{1}{2}Y_s \int_{S_s} E_{sx}^2\, da \tag{45}$$

and that by the surface wave by

$$P_d = \tfrac{1}{2}Y_d \int_{S'} E_{dx}^2\, da. \tag{46}$$

Inserting the approximate field expressions into the transmission integral, (39) then yields

$$T \simeq \frac{1}{4}\frac{w}{y_1}\left\{\left(\frac{\varepsilon_r}{\varepsilon_{\text{eff}}}\right)^{1/4} + \left(\frac{\varepsilon_{\text{eff}}}{\varepsilon_r}\right)^{1/4}\right\}^2. \tag{47}$$

Now, for a spatial variation in field strength throughout the resonator according to the factor

$$\cos\frac{m\pi z}{L}$$

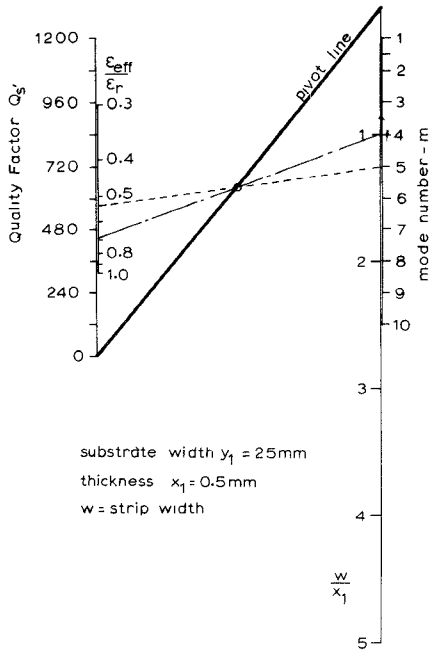

Fig. 8. Nomogram for the unloaded Q factor $Q_{s'}$ for *one* end of an open-ended microstrip resonator.

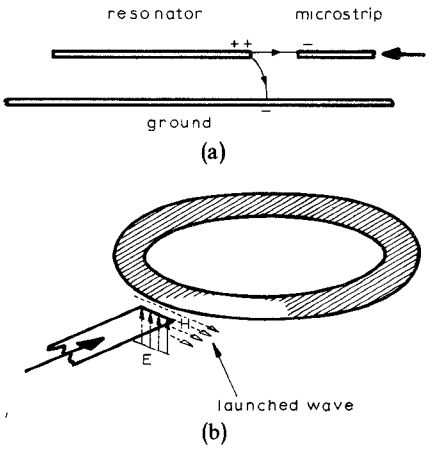

Fig. 9. Field perturbations due to coupling structures. (a) End-fed straight microstrip resonator. (b) Broadside-fed ring resonator.

where m is the mode number, the energy stored is twice the electric stored energy, i.e.,

$$\frac{\varepsilon_0 \varepsilon_r}{2} \int_0^{x_1} \int_{-w/2}^{w/2} \int_0^{L} E_{sx}^2 \, dv = \frac{\varepsilon_0 \varepsilon_r}{4} E_{sx}^2 x_1 w L. \tag{48}$$

The energy lost per cycle, at frequency f, to surface waves launched from *one* end of the resonator is

$$\frac{P_d}{f} = \frac{TP_s}{f} = \frac{TY_s E_{sx}^2 x_1 w}{2f}. \tag{49}$$

Hence from the defining relationship for Q, (38), we obtain

$$Q_{s'} = \frac{\pi f}{T} \frac{\varepsilon_0 \varepsilon_r}{Y_s} L. \tag{50}$$

Finally, after eliminating T using (47) and noting that

$$L = \frac{m\lambda_{\text{strip}}}{2} = \frac{m}{2} \frac{Y_{\text{free space}}}{\varepsilon_0 \sqrt{\varepsilon_{\text{eff}}} f} \tag{51}$$

there results

$$Q_{s'} \simeq 2\pi \cdot \frac{y_1}{w} \cdot m \frac{(\varepsilon_r/\varepsilon_{\text{eff}})^{1/2}}{\{1 + (\varepsilon_{\text{eff}}/\varepsilon_r)^{1/2}\}^2} \tag{52}$$

per end. A nomogram derived from this expression is given in Fig. 8. Its construction allows for the fact that, for any given values of (w/x_1) and m, $(\varepsilon_{\text{eff}}/\varepsilon_r)$ will vary with the length of the resonator (via the frequency f), as well as with the nature of the substrate material (alumina, sapphire, quartz, etc.). Thus in any practical problem it is necessary to have an estimate for $(\varepsilon_{\text{eff}}/\varepsilon_r)$ which takes account of these dependences, either by reference to published curves [5], [17]–[20], or by empirically deducing the wavelength in the microstrip. Appendix C describes the use of the chart.

The kind of end-fed resonator as used by Edwards [5] (Fig. 1(c)) would have a $Q_{s'}$ determined by one end (the free end) only; energy lost from the coupling end would count as energy transferred to the external circuit, and hence as part of the external Q. Thus, from the nomogram, we could expect $Q_{s'}$ values upwards of 50–100, depending upon the impedance of the line and the order of the mode. We have to compare this with the Q_s value.

A straightforward calculation using equations (18) and (40) yields $Q_s \simeq x_1/\delta \simeq 250$ at 1 GHz, using a typical value for the conductivity of electrodeposited copper [21]. Judging by the Q measured for resonators of the type shown in Fig. 1(b) [6], for which $Q_0 = Q_s$, the estimate of $Q_s = 250$ is probably very close to the practical values, yet values of $Q_0 \sim 100$ only are regularly measured for microstrip resonators. The suggestion is, therefore, that Q_0 is determined by $Q_{s'}$ and that correction of ε_{eff} (via ω) for Q_0 would lead to a value of $\varepsilon_{\text{eff}} \sim 1$ percent lower, whereas the true correction required is $\sim -1/250 \times 100$ percent $= -0.4$ percent, a figure which often may be considered negligible (Edwards [5], for example, took no account of resonator Q). In cases where it is thought necessary to account for Q_s, Q_s (proportional to $\sqrt{\omega}$) and $Q_{s'}$ (proportional to ω) could be separated by data analysis of a plot of Q_0^{-1} versus ω^{-1}.[4] Correction for Q_s in this way would lead to ε_{eff} values 0.5 percent lower at low frequencies, and less than that, by the factor $1/\sqrt{\omega}$, at higher frequencies, which affects the detailed shape of the dispersion curves [5].

B. Reactive-Only Perturbations

For microstrip resonators of the type shown in Fig. 1(c) there is only perturbation of the E field at either end of the strip. We may therefore apply the results of the fringing calculation carried out in Section II-B directly. The fringing field at the coupling end is slightly different from that at the free end insofar as some lines of E are drawn upwards to terminate on the feed microstrip (see Fig. 9(a)), so that the

[4] Currently the subject of experimental investigation.

Δ's will be different for each end. A figure for Δ at the free end for narrow strips (where (31) does not strictly apply) can be obtained from the literature [22]. For $(w/x_1) = 1$, for example,

$$\Delta = 0.35x_1.$$

Taking, depending upon the coupling gap width, $\Delta_g \simeq 1.2\Delta$ [23], we find from Table II (with $a = L =$ length of resonator)

$$\frac{\delta\varepsilon}{\varepsilon} \simeq +3.85 \text{ percent}$$

as the error arising from neglect of fringing and coupling in a 1-cm resonator on a 0.5-mm substrate. (Out of recognition of the likely magnitude of this error, Edwards *et al.* have recently published a technique whereby the total end-effect length represented by $(\Delta + \Delta_g)$ is experimentally eliminated between two resonators, one approximately twice the length of the other [5].)

The generality of the method as given in Section II-B, however, extends further in that it establishes semiquantitative correction procedures applicable to other launcher/resonator configurations. One such is the ring resonator (Fig. 9(b)), which is frequently employed in dispersion and other measurements. In this device we may regard the feed microstrip as launching a surface wave of the type considered in (41) into the side of the ring. This introduces a longitudinal $\boldsymbol{H}$ component into the microstrip-line of which the resonant ring is comprised, while for wide coupling gaps $\boldsymbol{E}$ is not greatly perturbed. From Table I we would then anticipate a small upward shift in ω, whose exact magnitude would depend upon the linewidths, ring diameter, and so on.

IV. Waveguide-Type Cavities

Cavities of this type have been used mainly in an effort to measure the substrate permittivity directly [1]–[4] and, to a lesser extent, the temperature coefficient of permittivity [6]. Both wholly (Fig. 1(b)) and partially (Fig. 1(a)) metallized resonators have been investigated.

A. Q_0-Associated Corrections

For all-over metallization, Q_0 $(= Q_s)$ values upwards of 250 normally are measured. For the open-edged resonators used in [1] and [3], unloaded Q values of $Q_0 \simeq 80$ and over have been obtained, so that, as in the microstrip resonator, Q_0 is dominated by $Q_{s'}$, except that here $Q_{s'}$ arises from energy lost by radiation into free space [24] instead of surface waves. Provided that the radiated waves introduce no phase shift into the fields existing at the walls S', however, the result that there is no first-order $Q_{s'}$-associated frequency shift will stand. Thus, regardless of whether the waveguide-type cavities have entirely electric walls or mixed boundary conditions, the Q_s is at least as high as that in microstrip resonators. Thus its neglect can be expected to lead to an error $\delta\varepsilon/\varepsilon < +0.4$ percent. In the experiments of [3] this is about one order of magnitude less than the largest error due to coupling perturbations. We therefore consider these next.

B. Reactive-Only Perturbations

In Fig. 10 we re-present the main results from [3], which show (in Fig. 10(b)) the experimental points averaged over 15 substrate samples. All of the modes indicated were excited in every sample. The open data points were obtained from transmission measurements on cavities with magnetic sidewalls, as in Fig. 1(a) with input/output coupling at diagonally opposite corners and the solid points from transmission measurements on resonators of the kind shown in Fig. 1(b), but with excitation via a broad-wall hole. In all cases the criterion for resonance was taken as the frequency of maximum transmission. The scatter in points is between 1 and 4 percent. We reexamine this data in the face of the criticism raised by Owens *et al.* [13].

From Section IV-A it is clear that Q_s-associated perturbations do not account for the scatter ($\delta\varepsilon/\varepsilon < +0.4$ percent). Similarly, from Section II-B it is equally clear that fringing does not account for the scatter either ($\delta\varepsilon/\varepsilon \simeq +0.64$ percent, independently of mode). (It should be remarked here that fringing is less severe than in microstrip resonators because the fields are more tightly bound to the cavity—there is no dielectric beyond the metallization.) We are therefore left with coupling errors.

Fig. 10(a) shows the theoretical scatter in points obtained by applying the methods given in Section II-B based upon the following premises: in the closed-wall resonators the $\boldsymbol{H}$ field at the broad wall is caused to loop by the feed line into a volume $\Delta\tau_e$ which is positive, while the electric field is essentially undisturbed; in the open-edged resonators the magnetic field at the corners (see Fig. 5) is largely undisturbed, while the $\boldsymbol{E}$ field is drawn out from a volume $\Delta\tau_m$, in the resonator corners, which is therefore negative. Except for the $(n,0)$ modes, which were explained adequately in [3], the relative placement of the error points is semiquantitatively correct. In this particular set of measurements, therefore, where the coupling was purposely tight enough to access all the modes with adequate sensitivity from the Hewlett Packard 8410A/8740A network analyzer used, the error was dominated by coupling perturbations. All other possible sources of error (Q and fringing) were consequently discarded in the analysis, which is the particular point of contention raised by Owens *et al.* [13].

The results of Fig. 10 do, in fact, bear reexamination, but not for these reasons. The principal assumption made in [3], and that which could attract the greatest criticism, was that the coupling volume $\Delta\tau$ was taken to be the same for both open-edged and closed-edged resonators, i.e., $\Delta\tau_e = \Delta\tau_m$. It is this assumption which can be challenged.

By careful comparison of (a) and (b) of Fig. 10, it can be seen that the scatter in experimental points for closed-wall resonators (the solid data) is slightly less than in the corresponding theoretical points, where equal $\Delta\tau$'s are assumed: they would have been more comparable had a smaller value of $\Delta\tau$ been used in predicting the upper half of

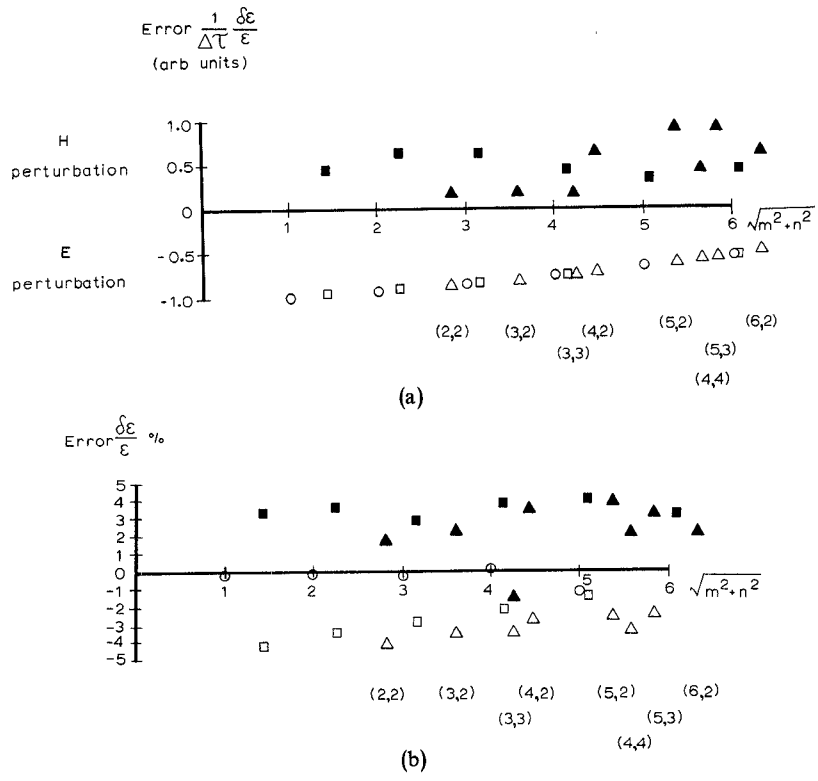

Fig. 10. Mode errors in ε_{xx} (from [3]). (a) Theoretical. (b) Experimental (averaged over 15 samples).

TABLE III

Revised permittivity values for SAPPHIRE (Crystalline Al_2O_3)

9.42(4)	(base plane)
11.59(3)	(c - axis)

the theoretical diagram than the lower half, i.e., $\Delta\tau_e < \Delta\tau_m$. If this is done it compresses all the solid points in Fig. 10(a) down toward the horizontal (zero) axis. The last step is then to compare the positions of the horizontal axes in (a) and (b) of Fig. 10; this shows that the zero error line in Fig. 10(b) is too low; it must be weighted upwards toward the closed-edge data set by 0.8–1 percent. Thus the previously published values for ε [3] must be increased by circa 0.9 percent. Applying this correction *per se* yields the revised values given here in Table III.

These figures now agree more closely with those of Fontanella *et al.* [25], Loewenstein *et al.* [26], and those adopted by Owens *et al.* [13]. The following error bounds apply: $\varepsilon_\perp + 0.1$ percent, -1.6 percent; $\varepsilon_\parallel + 0.2$ percent, -1.5 percent. They include the uncertainty in the correction procedure for coupling errors, the effects of Q_s and fringing, a $\pm 10°C$ change in temperature, and anisotropy, all as treated explicitly in this paper, together with instrument calibration error, an allowance for other (secondary) reactances associated with the coupling structures, mismatches in the input and output lines to the cavity, and, lastly, the precision of the measurement.[5]

Finally, we make the rather obvious remark that coupling errors can be reduced by firstly using a source/detector system allowing a higher insertion loss, and secondly contenting ourselves with exciting only those modes which couple most strongly, both of which enable the coupling volume to be decreased. Such techniques have been employed by Lenzing [2].

V. Conclusions

An MIC resonator with mixed boundary conditions, such as a microstrip resonator, loses energy at both imperfect electric and magnetic walls. There is a first-order shift in the resonant mode frequencies associated with the Q of the imperfect electric (metal) walls alone; magnetic walls introduce only a second-order shift. The latter may, however, dominate the unloaded Q, Q_0.

It has been shown that the effects of Q and reactive perturbations arising from fringing and coupling structures are the principal sources of error in resonance measurements for ε, or ε_{eff}. Such reactive effects may be treated

[5] It should be noted that, depending upon the criterion used to define resonance, different measured frequencies for any particular resonant mode will result if, firstly, reflection (or impedance) measurements are made as opposed to transmission measurements and, secondly, whereabouts in the feed line the measurement plane is chosen in the case of the reflection method. The author is grateful to one of the referees for suggesting that this point should be made.

semiquantitatively by applying Slater's perturbation theorem over the region where the field is perturbed. These procedures yield the following revised values for the crystal permittivity of sapphire (monocrystalline Al_2O_3) in the microwave region; $\varepsilon_{\|}$ (parallel to the c axis) = 11.6 (+0.2 percent, −1.5 percent); $\varepsilon_{\perp}$ (base plane) = 9.4 (+0.1 percent, −1.6 percent).

Appendix A
Resumé of Nomenclature [8]

Any general field $\boldsymbol{E}$ inside a cavity is assumed to be expanded as a sum of solenoidal functions $\boldsymbol{E}_a$ and irrotational functions $\boldsymbol{F}_a$, where a refers to the ath normal mode. Similarly, $\boldsymbol{H}$ is assumed to be expanded in terms of solenoidal functions $\boldsymbol{H}_a$. Thus the $\boldsymbol{E}_a$'s and $\boldsymbol{H}_a$'s satisfy

$$\nabla \times \boldsymbol{H}_a = k_a \boldsymbol{E}_a \qquad \nabla \times \boldsymbol{E}_a = k_a \boldsymbol{H}_a \tag{A1}$$

where $k_a = \omega_a \sqrt{\mu\varepsilon}$ is the propagation constant associated with the ath mode, ω_a. The functions are orthogonal, and are normalized as follows:

$$\int_V H_a^2 \, dv = \int_V E_a^2 \, dv = 1$$

where V is the volume of the cavity. Thus if we multiply the following expansion by $\boldsymbol{E}_a$ and integrate over V:

$$\boldsymbol{E} = \sum_a e_a \boldsymbol{E}_a + \sum_a f_a \boldsymbol{F}_a$$

we obtain the coefficients e_a as $\int_V \boldsymbol{E} \cdot \boldsymbol{E}_a \, dv$ etc. If electric walls are defined as surfaces S on which

$$\boldsymbol{n} \times \boldsymbol{E}_a = 0$$

and magnetic walls as surfaces S' on which

$$\boldsymbol{n} \times \boldsymbol{H}_a = 0$$

then $\nabla \times \boldsymbol{E}$ and $\nabla \times \boldsymbol{H}$ expand directly to

$$\nabla \times \boldsymbol{E} = \sum_a \boldsymbol{H}_a \left(k_a \int_V \boldsymbol{E} \cdot \boldsymbol{E}_a \, dv + \int_S (\boldsymbol{n} \times \boldsymbol{E}) \cdot \boldsymbol{H}_a \, da \right)$$

$$\nabla \times \boldsymbol{H} = \sum_a \boldsymbol{E}_a \left(k_a \int_V \boldsymbol{H} \cdot \boldsymbol{H}_a \, dv + \int_{S'} (\boldsymbol{n} \times \boldsymbol{H}) \cdot \boldsymbol{E}_a \, da \right)$$

where $\boldsymbol{n}$ is a normal directed out of V (i.e., into S,S').

By substituting these expansions into Maxwell's curl equations and equating coefficients, (7) and (8) of the text are obtained. These last two relations may be further combined to give

$$\begin{aligned} &\varepsilon\mu \frac{d^2}{dt^2} \int_V \boldsymbol{E} \cdot \boldsymbol{E}_a \, dv + k_a^2 \int_V \boldsymbol{E} \cdot \boldsymbol{E}_a \, dv \\ &\quad = -\mu \frac{d}{dt} \left(\int_V \boldsymbol{J} \cdot \boldsymbol{E}_a \, dv - \int_{S'} (\boldsymbol{n} \times \boldsymbol{H}) \cdot \boldsymbol{E}_a \, da \right) \\ &\qquad - k_a \int_S (\boldsymbol{n} \times \boldsymbol{E}) \cdot \boldsymbol{H}_a \, da \end{aligned} \tag{A2}$$

which is required for the derivation in Appendix B.

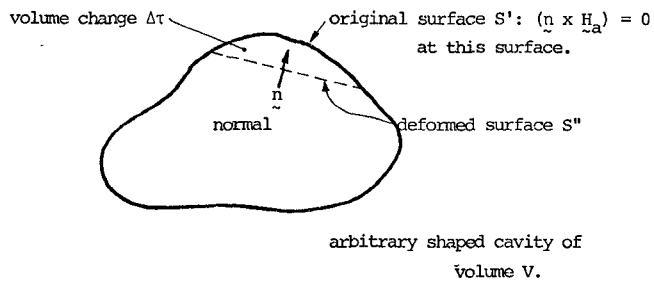

Fig. 11.

Appendix B
Slater's Perturbation Theorem for a Magnetic Wall

(This follows closely Slater's derivation for electric walls [8].)

Consider a cavity with some of its walls magnetic, and consider also part of one of these walls to be pushed-in slightly; see Fig. 11. Since the electric field within $\Delta\tau$ is now zero, there is a discontinuity in the tangential component of $\boldsymbol{E}$ at the perturbed wall. This corresponds to a (fictitious) surface current over S'' given by $(\boldsymbol{n} \times \boldsymbol{E})$, so we must consequently include a contribution

$$-\int_{S''} (\boldsymbol{n} \times \boldsymbol{E}) \cdot \boldsymbol{H}_a \, da$$

to the right-hand side of (A2).

For small deformations, the perturbed field $\boldsymbol{E}$ will very closely approximate the original field—which we assume to be the ath normal mode—multiplied by its coefficient $\int_V \boldsymbol{E} \cdot \boldsymbol{E}_a \, dv$; i.e., for the ath normal mode (or resonance) when the boundary is perturbed

$$\boldsymbol{E} \simeq \boldsymbol{E}_a \int_V \boldsymbol{E} \cdot \boldsymbol{E}_a \, dv$$

and hence

$$\begin{aligned} &-\int_{S''} (\boldsymbol{n} \times \boldsymbol{E}) \cdot \boldsymbol{H}_a \, da \\ &\quad = -\int_{S''} (\boldsymbol{n} \times \boldsymbol{E}_a) \cdot \boldsymbol{H}_a \, da \int_V \boldsymbol{E} \cdot \boldsymbol{E}_a \, dv \\ &\quad = -\int_{S''} \boldsymbol{n} \cdot (\boldsymbol{E}_a \times \boldsymbol{H}_a) \, da \int_V \boldsymbol{E} \cdot \boldsymbol{E}_a \, dv. \end{aligned} \tag{B1}$$

In order to simplify the surface integral, consider

$$\begin{aligned} \nabla \cdot (\boldsymbol{E}_a \times \boldsymbol{H}_a) &= \boldsymbol{H}_a \cdot (\nabla \times \boldsymbol{E}_a) - \boldsymbol{E}_a \cdot (\nabla \times \boldsymbol{H}_a) \\ &= k_a (H_a^2 - E_a^2) \end{aligned}$$

by (A1). Integrating both sides and applying the divergence theorem gives

$$\begin{aligned} \int_{\Delta\tau} \nabla \cdot (\boldsymbol{E}_a \times \boldsymbol{H}_a) \, dv &= k_a \int_{\Delta\tau} (H_a^2 - E_a^2) \, dv \\ &= -\int_{S' + S''} (\boldsymbol{E}_a \times \boldsymbol{H}_a) \cdot \boldsymbol{n} \, da \end{aligned}$$

where the minus sign on the right-hand side arises because $\boldsymbol{n}$ is directed *into* $\Delta\tau$. The surface integral may be split into two

parts: one over S' and one over S''. We may rewrite the integrand as $-\boldsymbol{n} \cdot (\boldsymbol{E}_a \times \boldsymbol{H}_a) = \boldsymbol{E}_a \cdot (\boldsymbol{n} \times \boldsymbol{H}_a) = 0$ (see the figure and the boundary conditions for S' stated in Appendix A), so we are left with

$$-\int_{S''} \boldsymbol{n} \cdot (\boldsymbol{E}_a \times \boldsymbol{H}_a)\, da = k_a \int_{\Delta\tau} (H_a^2 - E_a^2)\, dv. \quad \text{(B2)}$$

We now substitute (B2) into (B1) and add this term into the right-hand side of (A2) under the assumptions:

i) all other terms on the right-hand side of (A2) are zero;
ii) $\int_V \boldsymbol{E} \cdot \boldsymbol{E}_a\, dv$ = coefficient of $\boldsymbol{E}_a$, varies as $e^{j\omega t}$; ω = real.

This gives

$$-\omega^2 \mu\varepsilon + k_a^2 = k_a^2 \int_{\Delta\tau} (H_a^2 - E_a^2)\, dv$$

or, since $k_a^2 = \omega_a^2 \mu\varepsilon$ where ω_a is the frequency of the ath (unperturbed) normal mode,

$$\frac{\omega^2 - \omega_a^2}{\omega_a^2} = \int_{\Delta\tau} (E_a^2 - H_a^2)\, dv \quad \text{(B3)}$$

for, recall, a *decrease* in volume $\Delta\tau$.

The right-hand side is of opposite sign to that which results when an electric side wall is pushed in [8]. That this is correct may be checked against the expectation that, in either cavity type, ω should decrease for a small increase in resonator dimensions (refer to Table I of the text).

Appendix C
Use of the Nomogram (Fig. 8)

i) Determine an approximate value for $(\varepsilon_{\text{eff}}/\varepsilon_r)$ at the particular (w/x_1) and frequency of interest. Example:

$$\varepsilon_{\text{eff}} = 6.8 \qquad \varepsilon_r = 9.8 \qquad w/x_1 = 1.$$

ii) Draw a line (——·——·——) connecting the $(\varepsilon_{\text{eff}}/\varepsilon_r)$ value on the left-hand scales with the (w/x_1) value on the right-hand scales. Let this line intersect the "pivot line" at point 0.

iii) Draw a line (- - - - -) connecting point 0 with the mode number m on the right-hand scales, and extrapolate to cut the $Q_{s'}$ axis. Example:

$$m = 5 \quad \text{giving} \quad Q_{s'} = 576$$

per end, or 288 if there is loss from both ends of the resonator.

Acknowledgment

The author takes pleasure in acknowledging many helpful discussions on this subject with Dr. E. H. Fooks of the Department of Communications, University of New South Wales. T. C. Edwards is similarly thanked for a very helpful exchange of ideas on correspondence over references [3], [5], and [13].

References

[1] L. S. Napoli and J. J. Hughes, "A simple technique for the accurate determination of the microwave dielectric constant for microwave integrated-circuit substrates," *IEEE Trans. Microwave Theory Tech.*, vol. MTT-19, pp. 664–665, July 1971.
[2] H. F. Lenzing, "Measurement of dielectric constant of ceramic substrates at microwave frequencies," *Amer. Ceram. Soc. Bull.*, vol. 51, p. 361, 1972.
[3] P. H. Ladbrooke, M. H. N. Potok, and E. H. England, "Coupling errors in cavity-resonance measurements on MIC dielectrics," *IEEE Trans. Microwave Theory Tech.* (Short Paper), vol. MTT-21, pp. 560–562, Aug. 1973.
[4] J. Q. Howell, "A quick accurate technique to measure the dielectric constant of microwave integrated-circuit substrates," *IEEE Trans. Microwave Theory Tech.* (Short Paper), vol. MTT-21, pp. 142–143, Mar. 1973.
[5] T. C. Edwards and R. P. Owens, "2 to 18 GHz dispersion measurements on 10 to 100 ohm microstriplines on sapphire," *IEEE Trans. Microwave Theory Tech.*, vol. MTT-24, pp. 506–513, Aug. 1976.
[6] J. E. Aitken, P. H. Ladbrooke, and M. H. N. Potok, "Microwave measurement of the temperature coefficient of permittivity for sapphire and alumina," *IEEE Trans. Microwave Theory Tech.* (Short Paper), vol. MTT-23, pp. 526–529, June 1975.
[7] R. E. Collin, *Foundations for Microwave Engineering*. New York: McGraw-Hill, 1966.
[8] J. C. Slater, *Microwave Electronics*. Princeton, NJ: Van Nostrand, 1950.
[9] E. L. Ginzton, *Microwave Measurements*. New York: McGraw-Hill, 1957.
[10] P. H. Ladbrooke, "A novel standing-wave indicator in microstrip," *Radio and Electronic Engr.*, vol. 44, pp. 273–280, May 1974.
[11] J. R. James and P. H. Ladbrooke, "Surface-wave phenomena associated with open-circuited stripline terminations," *Electronics Letters*, vol. 9, pp. 570–571, Nov. 1973.
[12] R. Plonsey and R. E. Collin, *Principles and Applications of Electromagnetic Fields*. New York: McGraw-Hill, 1961.
[13] R. P. Owens, J. E. Aitken, and T. C. Edwards, "Quasi-static characteristics of microstrip on an anisotropic sapphire substrate," *IEEE Trans. Microwave Theory Tech.*, vol. MTT-24, pp. 499–505, Aug. 1976.
[14] J. H. C. van Heuven and T. H. A. M. Vlek, "Anisotropy in alumina substrates for microstrip circuits," *IEEE Trans. Microwave Theory Tech.* (Short Paper), vol. MTT-20, pp. 775–777, Nov. 1972.
[15] Y. Satomura, M. Matsuhara, and N. Kumagai, "Analysis of electromagnetic-wave modes in anisotropic slab waveguide," *IEEE Trans. Microwave Theory Tech.*, vol. MTT-22, pp. 86–92, Feb. 1974.
[16] H. M. Barlow and J. Brown, *Radio Surface Waves*. Oxford, England: Clarendon Press, 1962.
[17] E. Denlinger, "A frequency dependent solution for microstrip transmission lines," *IEEE Trans. Microwave Theory Tech.*, vol. MTT-19, pp. 30–39, Jan. 1971.
[18] W. J. Getsinger, "Microstrip dispersion model," *IEEE Trans. Microwave Theory Tech.*, vol. MTT-21, pp. 34–39, Jan. 1973.
[19] K. Mehmet, M. K. McPhun, and D. F. Michie, "Simple resonator method for measuring dispersion of microstrip," *Electronics Letters*, vol. 8, pp. 165–166, Mar. 23, 1972.
[20] J. Deutsch and H. J. Jung, "Measurement of the attenuation and effective dielectric constant of microstriplines in the frequency range between 2 and 12 GHz," in *Proc. 1971 European Microwave Conf.*, pp. C3/4: 1–4 (Stockholm, Sweden).
[21] P. H. Ladbrooke, E. H. England, and M. H. N. Potok, "A specific thin-film technology for microwave integrated-circuits," *IEEE Trans. Manuf. Tech.*, vol. MFT-2, pp. 53–59, Dec. 1973.
[22] D. S. James and S. H. Tse, "Microstrip end effects," *Electronics Letters*, vol. 8, pp. 46–47, Jan. 27, 1972.
[23] T. C. Edwards, "Microwave design parameters for microstrip transmission lines on sapphire substrates," M. Phil. dissertation, Royal Military College of Science, Shrivenham, unpublished.
[24] H. Sobol, "Radiation conductance of open-circuit microstrip," *IEEE Trans. Microwave Theory Tech.*, vol. MTT-19, pp. 885–887, Nov. 1971.
[25] J. Fontanella, C. Andeen, and D. Schuele, "Low-frequency dielectric constant of α-quartz, sapphire, MgF_2 and MgO," *J. Appl. Phys.*, vol. 45, pp. 2852–2854, July 1974.
[26] E. V. Loewenstein, D. R. Smith, and R. L. Morgan, "Optical constants for infra-red materials, 2: Crystalline solids," *Applied Optics*, vol. 12, pp. 398–406, Feb. 1973.